LABORATORI NAZIONALI DI FRASCATI
SIS – Pubblicazioni

LNF-02/017 (P)
9 Settembre 2002

LOCAL AND AVERAGE FE DISTRIBUTION IN TRIOCTAHEDRAL MICAS: ANALYSIS OF FE K-EDGE XANES SPECTRA IN THE PHLOGOPITE-ANNITE AND PHLOGOPITE-TETRA-FERRIPHLOGOPITE JOINS ON THE BASIS OF SINGLE-CRYSTAL XRD REFINEMENTS

Francesca Tombolini[1], Maria Franca Brigatti[2], Augusto Marcelli[1], Giannantonio Cibin[1], Annibale Mottana[3, 1], Gabriele Giuli[4]

[1)]INFN-Laboratori Nazionali di Frascati Via E. Fermi 40, I-00044 Frascati, Italy
[2)]Dipartimento di Scienze della Terra, Università di Modena e Reggio Emilia, Largo S. Eufemia 19, I-41100 Modena, Italy
[3)] Dipartimento di Scienze Geologiche, Università Roma Tre, Largo S. Leonardo Murialdo 1, I-00146 Roma, Italy
[4)] Dipartimento di Scienze della Terra, Università di Camerino, Via Gentile III da Varano, I-62032 Camerino, Italy

Abstract

In Fe-bearing trioctahedral micas Fe^{2+} occurs essentially in the octahedral O sheet whereas Fe^{3+} can either coexist with Fe^{2+} in the octahedral M sites or occur in tetrahedral T sites. Fe K-edge absorption spectra of twelve micas were recorded in an effort to relate their absorption features to the results of single-crystal X-ray structure refinements obtained on crystals from the same rock sample. This study involves the three end members phlogopite, annite and tetra-ferriphlogopite, used as reference materials, and nine micas intermediate in composition along the joins phlogopite-tetra-ferriphlogopite and phlogopite-annite. A detailed analysis of the XAS spectral features singles out the independent effects of coordination and valence shows and distinctly different position vs. intensity trends to be present that depend upon the local environment of Fe^{2+} and Fe^{3+}. Bond distances evaluated from XANES spectra at the edge, or FMS, region agree well with those obtained by X-ray diffraction refinement. Distinct variations in the local to intermediate ranges of order of certain micas are determined by the analysis of XANES, or IMS, regions; they supplement well the information on their long range orders best obtained by X-ray refinement.

PACS.: 61.10Ht (XAS),61.12.Ld (XRD),91.60.Ed (Geophys., crystal structure),70 (Cond.Matt.)

Submitted to European Journal of Mineralogy

1 INTRODUCTION

Iron is the most important transition element in trioctahedral micas. However, depending on redox conditions during crystallisation, the Fe^{2+}/Fe^{3+} ratio can vary significantly as does its distribution in the mica layered structure: Fe^{3+} can occupy both the tetrahedral (T) and octahedral (M) sites, whereas Fe^{2+} is assumed to occur only in octahedral sites.

Starting from the ideal phlogopite composition [$^{[12]}K\ ^{[4]}(Si_2Al)\ ^{[6]}Mg_3\ O_{10}\ (OH,\ F)_2$], the homovalent $^{[4]}Fe^{3+}$ for $^{[4]}Al^{3+}$ tetrahedral substitution, which gives way to the solid solution between phlogopite and tetra-ferriphlogopite, is considered to occur with a complete random distribution of Fe^{3+} in the T site. By contrast, the homovalent $^{[6]}Fe^{2+}$ for $^{[6]}Mg^{2+}$ substitution, which generates the join phlogopite-annite, occurs first in the M-*trans* site, and then, with increasing annite component, in both the octahedral M-*trans* and octahedral M-*cis* sites (Brigatti & Guggenheim, 2000). Furthermore, a variety of possible substitutions have been proposed to explain the substitution mechanisms of Fe^{3+} in the octahedral sites of micas. These include: *i*) the oxy-reaction $^{[6]}Fe^{2+}_{-1}OH^{1-}_{-1}{}^{[6]}Fe^{3+}O^{2-}$; ii) the trioctahedral *vs*. dioctahedral substitution of the form $^{[6]}Fe^{2+}_{-3}{}^{[6]}Fe^{3+}_{2}$ + (where refers to octahedral vacancies in the mica crystal structure), and *iii*) the celadonitic substitution $^{[6]}Fe^{2+}_{-1}{}^{[4]}Si^{4+}_{-1}{}^{[6]}Fe^{3+}{}^{[4]}Al^{3+}$, which involves tetrahedral and octahedral sheets at the same time (Dymek, 1983; Burt, 1988). However, there is no consensus regarding either the oxidation mechanism or the octahedral sites involved.

Many previous studies have discussed the presence and the extent of the tetrahedral Fe^{3+} substitution in trioctahedral micas by means of optical observations (i.e., reverse absorption[18,22,32]); wet-chemical analyses; Raman infrared, Mössbauer, and X-ray absorption spectroscopy[6,8,12,13,14,19,20,26,27,29,33] and crystal structure refinements [3,4,8,10,19,37]. However, few data concern the Fe^{3+}/Fe^{2+} distribution among the octahedral sites[3,13,14,34,35,38]. The investigation of Rebbert *et al.* [34] on synthetic annite and siderophyllite and that of Redhammer *et al.*[35] on annite synthesised at different at different oxygen fugacities concluded that the Fe-vacancy substitution plays the dominant role in the oxidation of synthetic annite. By contrast, Virgo & Popp[38] suggested the oxy-substitution as the one dominating the composition of natural igneous micas. Thus, even though the authors do not explicitly mention the octahedral site involved, we can infer that Fe-vacancy substitution mainly involves the octahedral *trans*-site, whereas the oxy-substitution may occur in both the octahedral *trans* and *cis* sites. Brigatti *et al.*[3], combining single crystal X-ray diffraction and Mössbauer spectroscopy studies, suggested that in Fe-rich phlogopite Fe^{3+} occupies the octahedral *cis*-sites, whereas Fe^{2+} can occur in both *trans*- and *cis*-octahedra.

The Fe pre-edge position, which is located at ~15-20 eV lower energy than the main *K*-edge crest of Fe [39] and is related to 1s->3d and 1s->4p transitions[11,24,40],was used to determine the redox state of Fe in several silicate minerals, including Fe-rich phlogopite (referred as biotite by Heald *et al.*[23]), amphiboles [9], olivines [16], and was recently systematically examined by Wilke *et al.* [41] for natural oxides, silicates, sulphates and carbonates characterised by a wide range of coordination environments for Fe. This study suggests that, in minerals containing both Fe^{2+} and Fe^{3+} in different site geometries, the evaluation of Fe^{2+}/Fe_{tot} ratio is more accurate when the effects of Fe coordination on both the centroid and the total pre-edge positions are being considered.

This study presents the results of a XANES investigation designed to clarify the presence and location of Fe^{2+} and Fe^{3+} in several trioctahedral micas having wide ranges of total iron content, Fe^{2+}/ Fe_{tot} ratio, and coordination. It aims at demonstrating that a great number of information on how Fe^{2+} and Fe^{3+} distribute locally in the different site geometries can be extracted from XANES spectra, even when recorded on mica powders. In addition, it also aims at showing the extent of local information gathered by XAS in relation to the long-range results of XRD studies.

2 MATERIALS AND METHODS

2.1 Samples

Table 1 lists all the trioctahedral mica samples used to characterise Fe in the four-fold and in six-fold coordination environments, the chemical formulae deduced from electron microprobe analysis as well as the localities where they are from. The reference column indicates previous crystal chemical studies achieved on crystals from the same locality and closely similar. In some cases, previous crystal structure refinements (*e.g.,* phlogopite from Franklin[20], New York) had been carried on the actual crystals a portion of which was used to obtain the powders for XAS experiments. Only the crystal chemical data relevant for the XANES spectra discussion that will follow are actually reported. The reader should refer to the original papers for published data, while the complete data set of unpublished crystal structure refinements can be obtained upon request from M.F.B.

2.2 Methods

To test the chemical homogeneity of all the mica samples used in XAS analysis, major element analyses were carried out on a large number of mica crystals using a wavelength-dispersive ARL-SEMQ electron microprobe (operating condition: 15 kV accelerating voltage, 15 nA sample current and defocused electron beam with about 3 mm spot size). The intra-granular compositional variation was within 3% of the estimated standard error, indicating a high degree of chemical homogeneity, and all chemical data were averaged. The chemical formulae reported in Table 1 are based on $O_{12-(x+y+z)}$ (where, x is OH, y is F, and z is Cl) and were obtained by combining the results of: *i*) microprobe analysis; *ii*) OH determination obtained by thermo-gravimetric analysis in a flow of Ar gas to minimize the reaction $2FeO + 2(OH) \rightarrow Fe_2O_3 + H_2 + O^{2-}$ using a Seiko SSC 5200 thermal analyser equipped with the quadrupole mass spectrometer ESS, GeneSys Quadstar 422 to analyse the gases evolved during thermal reactions; *iii*) Fe^{3+} chemical determination by a semi-microvolumetric method[28].

Single crystal X-ray diffraction data collection (obtained using a Siemens P4P rotating-anode single crystal diffractometer) as well as crystal structure refinement (in the space group *C*2/*m*) were carried out following the procedures described fromBrigatti *et al*.[2,4]. For each crystal, appropriate scattering fully ionised scattering factors were applied to the octahedral M1 and M2 sites and interlayer A site, whereas mixed scattering factors were assumed for the anion and tetrahedral sites.

TAB. 1 - List of samples used for the study, chemical composition and previous crystal structure studies of similar crystals.

Sample label	Species	Locality	Chemical formula	Reference
Phl Fr-1	Phlogopite	Franklin, New Jersey	$(Si_{3.12}Al_{0.88})\ (Al_{0.08}Fe^{2+}_{0.05}Ti_{0.01}Mg_{2.85})\ (Na_{0.01}K_{1.00})\ O_{10.22}\ (OH)_{0.46}\ F_{1.31}\ Cl_{0.01}$	(1)
120	Annite	Pikes Peak, Colorado (USA)	$(Si_{3.14}Al_{0.86})\ (Al_{0.13}Fe^{3+}_{0.21}Fe^{2+}_{2.29}Mg_{0.10}Mn_{0.01}\ Ti_{0.25})\ (K_{0.99}Na_{0.01})\ O_{10.95}\ (OH)_{0.79}\ F_{0.26}$	Brigatti et al., 2000
Tas 22-1	Tetra-ferriphlogopite	Tapira (Brazil)	$(Si_{3.05}Fe^{3+}_{0.95})\ (Fe^{3+}_{0.08}Fe^{2+}_{0.17}Ti_{0.01}Mg_{2.73})\ (Na_{0.01}K_{0.99})\ O_{10.17}\ (OH)_{1.79}\ F_{0.04}$	Brigatti et al., 1996
Tpq 16-6	Tetra-ferriphlogopite	Tapira (Brazil)	$(Si_{3.15}Al_{0.04}Fe^{3+}_{0.81})\ (Fe^{3+}_{0.23}Fe^{2+}_{0.20}Ti_{0.02}Mg_{2.54})\ (Na_{0.02}K_{0.95})\ O_{10.34}\ OH_{1.56}\ F_{0.10}$	Brigatti et al., 1996
Wa 8h	Magnesian annite	Warburton, Lachlan Fold Belt (Australia)	$(Si_{2.82}Al_{1.18})\ (Al_{0.18}Fe^{3+}_{0.13}Fe^{2+}_{1.20}Ti_{0.29}Mg_{1.19}\ Mn_{0.02})\ (Ca_{0.03}Ba_{0.02}Na_{0.03}K_{0.89})\ O_{10.76}\ (OH)_{1.05}\ F_{0.14}\ Cl_{0.05}$	Brigatti et al., 1998
BHG-1	Ti-rich ferroan phlogopite	Black Hill (South Australia)	$(Si_{2.73}Al_{1.27})\ (Al_{0.13}Fe^{2+}_{1.00}Ti_{0.40}Mg_{1.14})\ (Ba_{0.01}Na_{0.01}K_{0..99})\ O_{10}\ (OH, F, Cl)_2$	(1)
19	Ferroan phlogopite	Euganean Hills (Italy)	$(Si_{2.75}Al_{1.25})\ (Al_{0.02}Fe^{3+}_{0.39}Fe^{2+}_{0.60}Ti_{0.37}Mg_{1.61}\ Mn_{0.01})\ (Ba_{0.03}Na_{0.07}K_{0..90})\ O_{10.93}\ (OH)_{0.84}\ F_{0.23}$	Brigatti & Poppi, 1993
Tag 15-3	Ferroan phlogopite	Tapira (Brazil)	$(Si_{2.74}Al_{1.15}Fe^{3+}_{0.11})\ (Fe^{3+}_{0.25}Fe^{2+}_{0.34}Ti_{0.13}Mg_{2.19}\ Mn_{0.01})\ (Ba_{0.02}K_{0.92})\ O_{10.04}\ (OH)_{1.91}\ F_{0.05}$	Brigatti et al., 1996
Tag 15-4	Ferroan phlogopite	Tapira (Brazil)	$(Si_{2.76}Al_{1.17}Fe^{3+}_{0.07})\ (Fe^{3+}_{0.23}Fe^{2+}_{0.38}Ti_{0.13}Mg_{2.25}\ Mn_{0.01})\ (Ba_{0.03}Na_{0.02}K_{0.95})\ O_{10.27}\ (OH)_{1.68}\ F_{0.05}$	Brigatti et al., 1996
Tai 17-1	Ferroan phlogopite	Tapira (Brazil)	$(Si_{2.82}Al_{1.10}Fe^{3+}_{0.08})\ (Fe^{3+}_{0.10}Fe^{2+}_{0.44}Ti_{0.09}Mg_{2.36}\ Mn_{0.01})\ (Ba_{0.01}Na_{0.02}K_{0.98})\ O_{10.12}\ (OH)_{1.88}$	(1)
Tae 23-1	$^{[VI]}Fe^{3+}$-containing Phlogopite	Tapira (Brazil)	$(Si_{2.82}Al_{1.13}Fe^{3+}_{0.05})\ (Fe^{3+}_{0.22}Fe^{2+}_{0.09}Ti_{0.09}Mg_{2.60})\ (Ba_{0.01}Na_{0.05}K_{0.88})\ O_{10.18}\ (OH)_{1.81}\ F_{0.01}$	Brigatti et al., 1996
Phl-2a	$^{[VI]}Al^{3+}$-containing Phlogopite	Mt. Monzoni (Italy)	$(Si_{2.60}Al_{1.40})\ (Al_{0.18}Fe^{3+}_{0.15}Fe^{2+}_{0.03}Ti_{0.01}Mg_{2.63})\ (Ba_{0.01}Na_{0.02}K_{0.95})\ O_{9.93}\ (OH)_{1.96}\ F_{0.11}$	Alietti et al., 1995

(1) Note: the complete, unpublished, crystal structure refinement is available on request.

X-ray absorption experiments were performed at Stanford Synchrotron Radiation Laboratory (SSRL) with the electron-storage ring operating at 3 GeV and electron current between 100 and 60 mA. Fluorescence-yield *K*-edge spectra were recorded for Fe at beam line SBO4-1, which is equipped with a double-crystal Si (111) monochromator having a resolution of ~1.5 eV. Spectra were recorded at steps of 0.35 eV for 1 s using a Lytle detector[25] with Soller slits, and with the sample compartment filled by N_2. Small amounts of powder of each sample were spread on transparent Kapton tape and mounted on the sample holder at 45° from the impinging beam. Data were collected at room temperature in air. Calibration for energy was made with a standard Fe metal foil.

The recorded spectra were energy-corrected as a function of the ring current, fitted with a Victoreen polynomial function to account for the base line, and normalised to 1 at high energy (50 eV above threshold[1]).

3 RESULTS AND DISCUSSION

We investigated trioctahedral micas where iron can be present in two different oxidation states (Fe^{2+}, Fe^{3+}) and coordinations (IV and VI).

In the micas from Tapira, Brazil (Table 1), both Al and Fe^{3+} replace Si^{4+} in the tetrahedral site ($^{[4]}Al^{3+}$, $^{[4]}Fe^{3+}$ <=> $^{[4]}Si^{4+}$), and the $^{[4]}Fe^{3+}$:$^{[4]}(Fe^{3+}+Al)$ ratios vary from 0.04 in sample Tae23-1 to 1.0 in sample Tas22-1, that is a natural tetra-ferriphlogopite end member. Unfortunately, the solid solution between the $^{[4]}Fe^{3+}$-bearing but poor phlogopite and tetra-ferriphlogopite is incomplete, so that, up to date, no X-ray study of a sample intermediate in composition could be made.

On the basis of bulk chemical considerations (Table 1), Mg ($^{[6]}$Mg), Fe ($^{[6]}$Fe), and Ti ($^{[6]}$Ti) represent the main octahedrally coordinated cations in the examined sample set. The amount of $^{[6]}Fe^{2+}$ varies from 0.017 (the phlogopite sample Phl Fr-1) to 0.766 (annite 120) over a total octahedral occupancy of 3.000, and in a few crystals some Fe^{3+} too occupies octahedral positions. The full compositional variation of the studied micas is complex, and complicates the description of the mechanisms governing the crystal chemistry of the octahedral layer. However, the main exchange mechanisms by which Fe increases its level on layer occupancy (in addition to the homovalent substitutions $^{[4]}Fe^{3+}$ $^{[4]}Al^{3+}_{-1}$ and $^{[6]}Fe^{2+}$ $^{[6]}Mg^{2+}_{-1}$ which link phlogopite to tetra-ferriphlogopite and phlogopite to annite, respectively) can be identified in the heterovalent exchange vectors $^{[6]}Fe^{3+}_{2}$ $^{[6]}$ $^{[6]}Mg^{2+}_{-3}$, $^{[6]}(Mg, Fe)^{2+}_{-1}$ $^{[4]}Si^{4+}_{-1}$ $^{[6]}Fe^{3+}$ $^{[4]}Al^{3+}$, and $^{[6]}Fe^{2+}_{-1}$ $(OH)^{-}_{-1}$ $^{[6]}Fe^{3+}$ O^{2-}. Thus, differences in the octahedral sheet chemistry are mostly accomplished by tetrahedral ring distortions instead of changes in the tetrahedral site dimensions; in turn, spectral changes observed in our XAS investigation are related to both the geometrical changes undergone by the structure and the Fe content of the mica samples.

In Fig. 1 we show the XANES Fe *K*-edge spectra of all the trioctahedral micas listed in Table 1.

In the upper part of the figure, we display for direct comparison the XANES spectra of samples compositionally close to end member compositions (phlogopite: Phl Fr-1, annite: 120,

tetra-ferriphlogopite: Tas 22-1). They have the maximum differences in the total amounts of Fe in the octahedral plane and in tetrahedrally coordinated Fe, respectively.

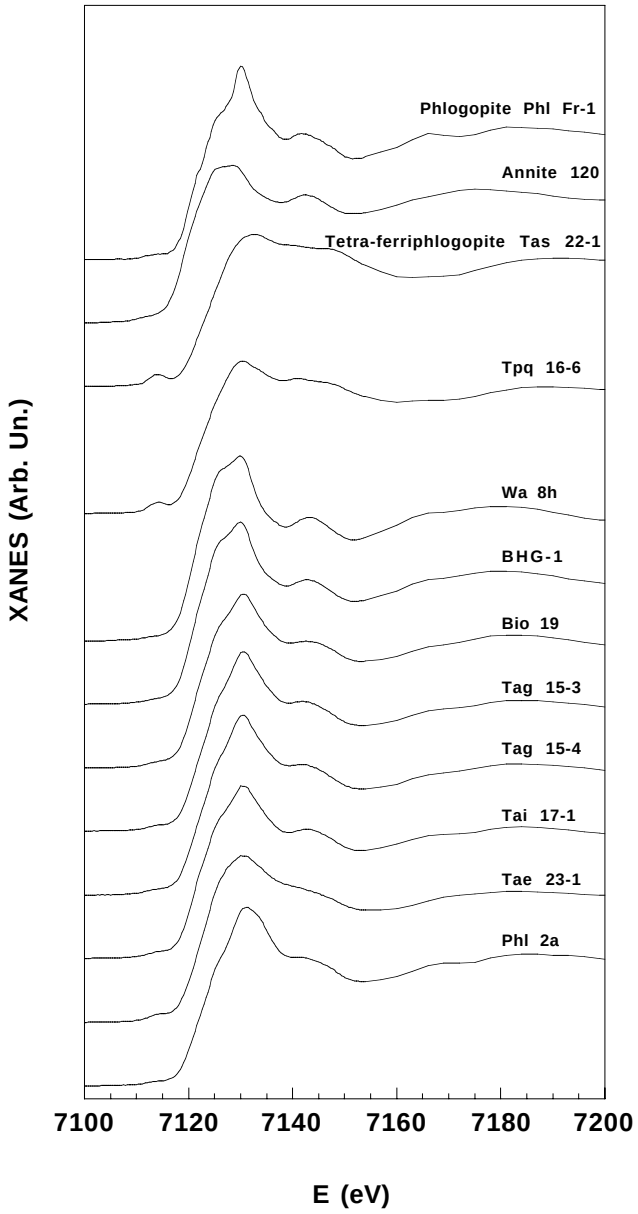

FIG. 1: *K*-edge XANES spectra of trioctahedral micas divided in two groups (top: end members, bottom: intermediate composition members in decreasing order of iron content. In between the two groups, the Tpq 16-6 sample – see text).

The Tas22-1 XANES spectrum shows, in addition to the maximum intensity in pre-edge A, which evidences the presence of Fe in tetrahedral coordination[15], an evident high complexity of the edge, or FMS, region. This region consists of several features up to 20 eV over the edge[31], and is followed by a broad, less defined series of multiple scattering (MS) contributions

in the XANES s.s. or IMS, region that reaches up to 50-60 eV above threshold. In Tas 22-1, the presence of a high Fe^{3+} amount in a unique location in the tetrahedral sheet (where normal micas would have Si or, possibly, Al) and of little Fe^{2+} in the octahedral sheets of the mica TOT layer determines a high level of structural disorder, which reflects into the XAS spectrum with broad features due to the overlapping of a multitude of MS contributions arising from the great number of Fe-O distances in both four-fold and six-fold coordination. Further on this can be found in Dyar *et al.*[15] and Giuli *et al.*[19]. The results from structure refinement support this interpretation, because they suggest M-O distances much larger than usual reflecting by the unusual lateral size of the tetrahedral sheet, thus increasing thermal vibration and distances between the octahedrally coordinated cations.

The two other samples at the top of Fig. 1, phlogopite Phl Fr-1 and annite 120, represent two opposite models of octahedral Fe occupancy in the O sheet. This is almost entirely consisting of Mg in the former sample (the little photoabsorbing Fe atom being distributed sparsely everywhere surrounded by Mg atoms), and of Fe in the latter one, where the photoabsorbing Fe atom is mostly surrounded by other Fe atoms. As a result, the phlogopite Phl Fr-1 XANES spectrum shows a completely different series of characteristics with respect to the tetra-ferriphlogopite Tas 22-1 one, and should be interpreted (following the Brigatti-Guggenheim model[2] based on XRD structure refinement) as being the typical Fe *K*-edge spectrum of a mica having diluted Fe^{2+} located in the M1 site only. Indeed, the spectrum shows a well defined series of features, indicating that Fe occurs in a quite ordered site distribution in the octahedral sheet; probably the most ordered one in the whole sample series. Conversely, in annite 120, the very high Fe concentration in an almost pure ferrous octahedral sheet determines large spectral variations with respect to phlogopite, which are evident both at the edge and in the IMS region. Moreover, the broad spectrum suggests Fe not to be ordered over the entire octahedral sheet, including the M2 site, in the sense that it reflects a structural disorder due to a great number of Mg-Fe(M1)-Fe(M2) neighbour configurations. Finally, if compared to phlogopite, all features in the annite spectrum appear to be less defined and such features as D and E are both less defined and shifted to lower energy. The latter feature indicates that in phlogopite Fe is located in a M1 site which is significantly smaller than the average <M1-M2> site in annite, in agreement with the much lower <M1-O> average distance measured by XRD.

In the lower part of Fig.1 we report the whole spectra of micas arranged from top to bottom with increasing total iron contents. Note that such an order follows approximately the order of decreasing α (Table 2) i.e., the tetrahedral rotation angle that indicates how the overall distortion of the tetrahedral plane is affected by the presence of Fe and is due essentially to the mismatch between the tetrahedral and octahedral network sizes.

TABLE 2

	Phl Fr-1	120	Tas 22-1	Tpq 16-6	Wa 8H	BHG 1	19	Tag 15-3	Tag 15-4	Tai 17-1	Tae 23-1	Phl 2a
Unit cell parameters												
a(Å)	5.309(1)	5.384(1)	5.362(1)	5.356(1)	5.344(1)	5.391(2)	5.331(1)	5.329(2)	5.332(1)	5.3355(8)	5.330(2)	5.305(2)
b(Å)	9.189(1)	9.324(1)	9.288(1)	9.284(2)	9.258(1)	9.283(2)	9.230(2)	9.228(2)	9.230(2)	9.2457(7)	9.230(3)	9.189(3)
c(Å)	10.150(2)	10.254(1)	10.321(2)	10.309(3)	10.232(1)	10.223(2)	10.160(2)	10.258(3)	10.267(2)	10.294(2)	10.256(4)	10.286(3)
β(°)	100.08(1)	100.86(1)	99.99(1)	100.03(2)	100.15(1)	100.38(4)	100.19(1)	100.03(3)	99.99(2)	99.94(1)	99.92(3)	99.96(2)
Tetrahedral mean bond lengths and distortion parameters												
<T-O> (Å)	1.650(2)	1.658(2)	1.680(2)	1.673(2)	1.659(2)	1.663(2)	1.657(3)	1.658(3)	1.662(2)	1.665(2)	1.658(3)	1.663(2)
TAV (°^{2})	1.74	0.61	0.20	0.62	0.61	0.81	0.31	1.09	1.30	1.54	0.92	0.51
α (°)	6.7	1.51	11.5	10.2	7.04	5.8	7.6	8.5	9.1	9.0	8.9	11.1
Volume (Å^3)	2.30	2.34	2.43	2.40	2.34	2.36	2.32	2.34	2.35	2.37	2.34	2.36
Octahedral mean bond distances and distortion parameters												
<M1-O> (Å)	2.061(2)	2.117(2)	2.086(1)	2.091(2)	2.091(2)	2.109(2)	2.083(3)	2.085(3)	2.082(3)	2.084(1)	2.079(3)	2.067(2)
OAV_{M1} (°^{2})	41.97	33.65	37.22	33.91	38.30	42.08	38.81	32.52	33.19	33.32	33.43	37.87
$Volume_{M1}$ (Å^3)	11.45	12.46	11.91	12.0	11.98	12.27	11.53	11.90	11.85	11.88	11.80	11.57
<M2-O> (Å)	2.062(1)	2.098(2)	2.086(1)	2.089(2)	2.076(2)	2.083(2)	2.064(2)	2.078(4)	2.079(2)	2.081(2)	2.078(3)	2.064(2)
OAV_{M2} (°^{2})	42.86	28.84	37.49	33.67	34.42	35.21	43.6	31.2	32.38	32.87	33.65	37.42
$Volume_{M2}$ (Å^3)	11.46	12.14	11.90	11.97	11.75	11.86	11.81	11.80	11.81	11.8	11.79	11.51
Interlayer cation mean bond distances												
<A-O> inner	2.986(2)	3.143(2)	2.932(2)	2.955(2)	3.010(2)	3.040(3)	2.976(3)	2.977(4)	2.965(3)	2.973(2)	2.974(2)	2.927(2)
<A-O> outer	3.292(2)	3.212(2)	3.462(2)	3.422(2)	3.332(2)	3.309(3)	3.325(3)	3.365(4)	3.378(3)	3.382(2)	3.380(2)	3.429(2)

Notes: α (tetrahedral rotation angle) $=\Sigma_{i=1}^{6} \alpha_i/6$ where $\alpha_i = |120° - \phi_i|/2$ and where ϕ_i is the angle between basal edges of neighboring tetrahedra articulated in the ring; $\Delta z = [z_{(Obasal)max} - z_{(Obasal)min}]$ [cs*in*β]; TAV (tetrahedral angle variance) $=\Sigma_{i=1}^{3} (\vartheta\text{-}109.47°)^2/5$ and OAV (octahedral angle variance) $=\Sigma_{i=1}^{12} (\vartheta\text{-}90°)^2/11$ (Robinson et al., 1971).

In between the top and bottom series, Fig. 1 singles out the spectrum of mica Tpq16-6. Indeed this spectrum has some peculiar characteristics which set it in an intermediate position between tetra-ferriphlogopite Tas22-1 and all other Fe-rich samples, namely: (*i*) a fairly strong pre-edge A, suggesting the presence of a significant tetrahedral Fe^{3+} component, which is also confirmed by the chemical formula (Table 1) and by the single-crystal X-ray refinement [5)], (*ii*) a fairly broad edge crest and (*iii*) two features in the IMS region, which is essentially the same as that observed in Tas 22-1. Spectral differences between samples which display bulk chemical similarities are common in XAS studies and, actually, represent the key to interpret their physical differences in terms of local electronic properties. Indeed, such spectral differences lie not so much on chemistry, but mainly on the structural and electronic properties of the photoabsorbing atom in the investigated compound; explanations must be painstakingly sought by trial and error.

To extract information on the local structures of even more complex systems such as intermediate micas are, we will proceed stepwise, and start by investigating the XANES spectra of some model micas where Fe is mainly in octahedral coordination, separately from others where it occurs in tetrahedral coordination and from the overall group: in other words, we will now leave end member phlogopite and tetra-ferriphlogopite (see above, and Giuli *et al*., 2001) and study first the phlogopite to annite binary join by analysing both Fe^{2+}- and Fe^{3+}-bearing samples. We shall return to the phlogopite-tetra-ferriphlogopite join later, when the octahedral layer occupancy is clarified.

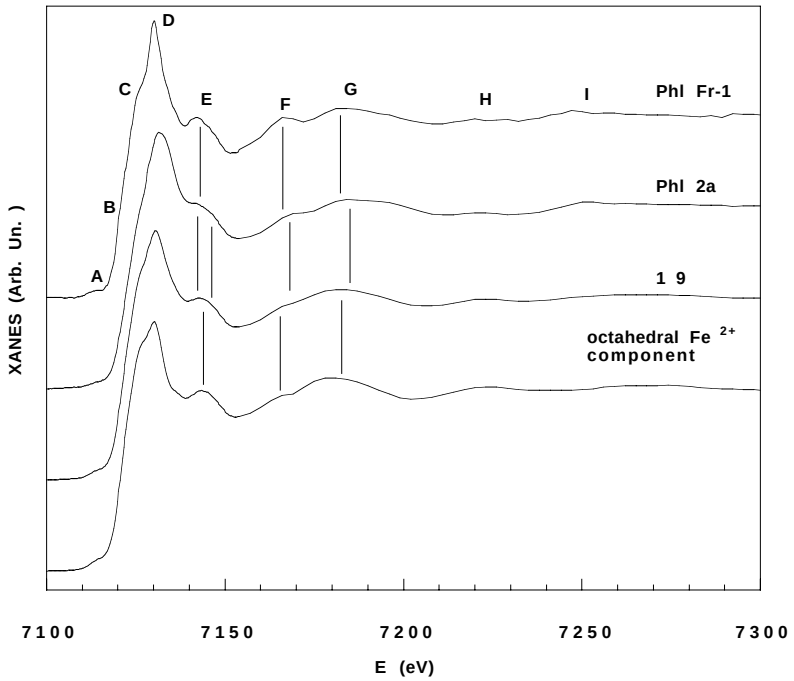

FIG. 2: Top: Fe *K*-edge XANES spectra of phlogopites Phl Fr-1, Phl 2a and of biotite 19. Bottom: the Fe^{2+} component of the biotite 19 XANES spectrum extracted considering Phl 2a as the pure Fe^{3+}-bearing model compound; note the similarity with the Phl Fr-1 spectrum, also due to Fe^{2+} only - see text for details

Fig. 2 analyses for comparison the Fe composition of the octahedral sheet of Phl Fr-1 and Phl-2a i.e., the phlogopites having the lowest total iron content in the whole series, which we consider to be model compounds for Fe distribution in a mica structure with overwhelming Mg environment. Direct comparison of their XANES spectra points out marked differences occurring in terms of large energy shifts at the main edge and of significant broadening in the MS region, respectively. In the edge region we note a definite energy shift (+ 1 eV) of the Phl-2a absorption edge with respect to Fr-1, together with a sequence of generally much broader features. The Phl Fr-1 spectrum displays an intense C shoulder on the lower energy limb of the main absorption edge D that is attenuate to almost disappear in the Phl-2a spectrum. In contrast, Phl-2a shows a clear splitting of the E feature and positive energy shifts of the F and G features. In these samples, the main edge shift can be directly correlated with their different oxidation states of Fe, thus confirming the presence of significant Fe^{3+} in Phl-2a and that essentially complete of Fe^{2+} in Phl Fr-1 which result from chemical analyses and single-crystal XRD refinements (Table 1). The observed differences in the IMS region (energy positions of F and G) reflect bond length and angle variations, which affect the MS paths to the Fe octahedral sites. On the basis of Natoli's (1983) well-known "thumb" rule, they may be explained in terms of a decrease of Fe-O averaged distances, thus supporting independently the previous inference that Fe^{3+} mainly occupies the M2 site, while Fe^{2+} occupies only the M1 site.

Extending now this inference to all mica samples, we suggest that an increase of Fe located in octahedral sites produces an increase in the mean electron counts of both the *trans*- (M1) and *cis*- (M2) octahedral sites, in moving along the join from phlogopite to annite through ferroan phlogopite and magnesian annite. This implies that an increase in the $Mg_{-1}Fe$ exchange occurs in both the M(1) and M(2) sites (Brigatti & Guggenheim, 2000). However, the ferroan phlogopite and magnesian annite samples in our investigated series (Fig. 1) show additional differences that may be related to differences in mean bond length existing between the M1 and M2 sites. Thus, a slight site preference of the large cation (i.e., Fe^{2+}) for M1, and of the small one (i.e., Fe^{3+} but also other cations such as Al^{3+}) for M2 can be surmised.

Biotite 19 XRD refinement data show a high octahedral iron total amount, however in mixed oxidation (i.e., both Fe^{2+} and Fe^{3+} are present, the Fe^{3+}/Fe^{2+} ratio being the highest (5:1) in the entire mica series), while the tetrahedral iron content is zero (Table 1). Indeed, this is also confirmed by the absolute absence of any pre-edge in the XANES spectrum (Fig. 2). Therefore, let's assume the Phl-2a spectrum as the model spectrum for almost pure Fe^{3+}-bearing mica and try to extract the Fe^{2+} spectral component of Bio 19 by subtracting from it the Phl-2a spectrum. The "virtual" Fe^{2+} spectrum resulting from such a difference (weighted according to the Fe^{2+}/Fe^{3+} concentration ratio) shows the same separation of the main edge in two components (B and C) as observed in Phl Fr-1, and in addition a general edge shift towards lower energies well seen in the energy position of the F and G features. Consequently, as a first approximation, we may consider the Bio19 Fe *K*-edge spectrum to be resulting from the linear combination of the Fe^{2+} and Fe^{3+} spectral components. In turn, this result suggests that, at moderate concentrations such as these, Fe be mainly distributed in M1 and M2 sites not yet perturbed by the presence of neighbour Fe atoms. Furthermore, the extracted spectrum edge position coincident to that of Fe^{2+} in Phl Fr-1 and the M1-like features at the same energies as in

the model compound would also indicate that during Fe oxidation an ordered distribution sequence is followed in micas: Fe^{2+} fills the M1 sites first and Fe^{3+} then enters the M2 sites.

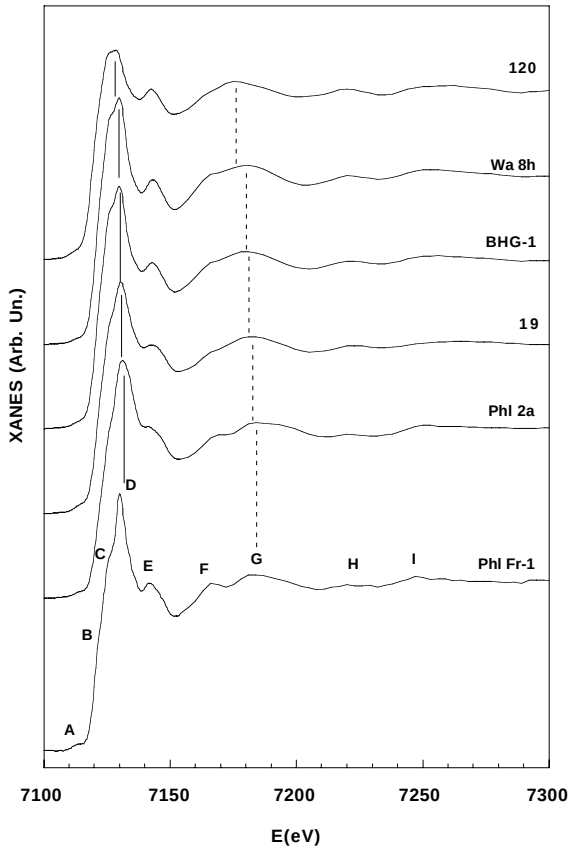

FIG. 3 Comparison among micas containing Fe in octahedral coordination. Note the highly ordered structure of the Phl Fr-1 spectrum, and the changes in intensity of the E feature and the shifts in energy of G feature over the series.

Fig. 3 displays the Fe *K*-edge XANES spectra of all the micas where Fe is in octahedral coordination. The general shape of all spectra is similar, however with small but significant differences. Clearest differences occur at the edge, where at least three contributions (B, C, and D) can be recognised. The C/D intensity ratio increases according to the total amount of iron determined in the samples (Table 1). Other, more subtle differences are present in the IMS region, where at least five features can be recognised (E, F, G, H, I): broadening of these features suggests that the configurations probed by the photoelectron increase at random so that structural disorder increases in the series from Fe-poor to Fe-rich micas i.e., from phlogopite Phl Fr-1 to annite 120. A monotonically decreasing behaviour is evidently followed by the G feature energy position, and corresponds to a monotonous, continuous increase of the average Fe octahedral size. Such an energy reduction, much higher than the one observed when

comparing the Phl Fr-1 vs. Phl-2a samples (see above), evidently reflects not so much a different M1 (large site) vs. M2 (small site) preferred occupation, rather the average size of the sites themselves. Indeed, in samples where Fe is present in minimum concentrations the Fe site size (which is the one measured by XRD refinement) is strongly influenced by the presence of mainly Mg in the adjacent sites of the octahedral network, thus determining the possible Fe site configurations, and in such a case we could identify and separate the M1 vs. M2 occupations, in Phl Fr-1 and Phl-2a, respectively. In other, Fe-richer samples the Fe-Fe octahedra interaction allows a more efficient deformation of the octahedral network, resulting in an average Fe site with greater M-O distances.

In contrast to what turns out from analysis of the IMS region, at the edge viz. FMS region the absorption edge position appears to follow the $Fe^{2+}/(Fe^{3+}+Fe^{2+})$ ratio almost independently from the total iron content, albeit with a marked change in slope from Fe-poor (right) to Fe-rich (left) micas (Fig. 4). This behaviour is in substantial agreement with the XRD data on the Fe^{3+} vs. Fe^{2+} concentrations (see Table 1). Another evidence to be detected in the FMS region is that the E feature characteristically broadens with decreasing Fe^{3+} content in all these micas (see also Fig. 2). However, this trend cannot be precisely quantified, nor is confirmed by the phlogopite Phl Fr-1 spectrum.

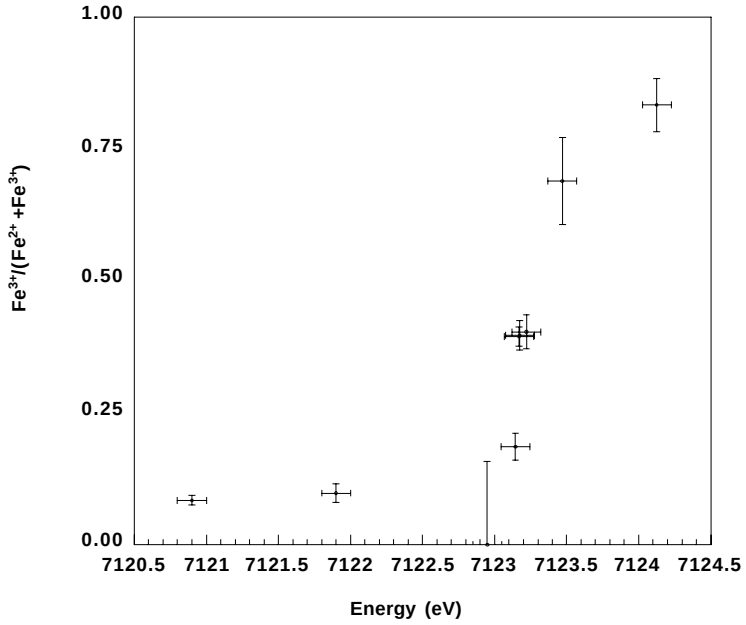

FIG. 4: The relationship between edge energy position and Fe oxidation ratio across the trioctahedral mica series.

We can now go back to the phlogopite-tetra-ferriphlogopite join and analyse it in detail according to the strategy sketched above: we will first study the spectral features of some model micas so as to extract their tetrahedral components, then apply these results to similar micas for

confirmation and, finally, extend our findings to the entire mica set. End member Tas22-1 and ferroan Tpq16-6 are our model tetra-ferri-phlogopite micas (Fig. 5). In the hypothesis that these samples have their spectra generated by Fe in octahedral and tetrahedral coordination similar and that they can be linearly combined, we can solve the spectral mixture that produces the complete XANES cross section of the mica and obtains the tetrahedral and octahedral components using the following linear system of two equations:

$$\begin{cases} \sigma_{tas} = \alpha\sigma_{comp.octahedr.tas} + \beta\sigma_{comp.tetrahedr.tas} \\ \sigma_{tpq} = \lambda\sigma_{comp.octahedr.tpq} + \mu\sigma_{comp.tetrahedr.tpq} \end{cases} \quad (1)$$

where the coefficients α, β, λ and μ are the atomic ratios in the chemical formulae of Table1. The remaining spectrum is the tetrahedral Fe component (Fig. 5) obtained by this simple approach. Feature E at 7147 eV is due only to the significant amount of Fe in tetrahedral coordination present in both Tas 22-1 and Tpq 16-6, whereas the weak peak D at 7141 eV shoul be essentially associated with the octahedral Fe component. Indeed, this assignment finds support in a simple comparison with the Phl Fr-1 spectrum (where Fe is entirely in octahedral coordination): the sharp feature E of it (Fig. 3) lies at the same energy position as D in Fig. 5.

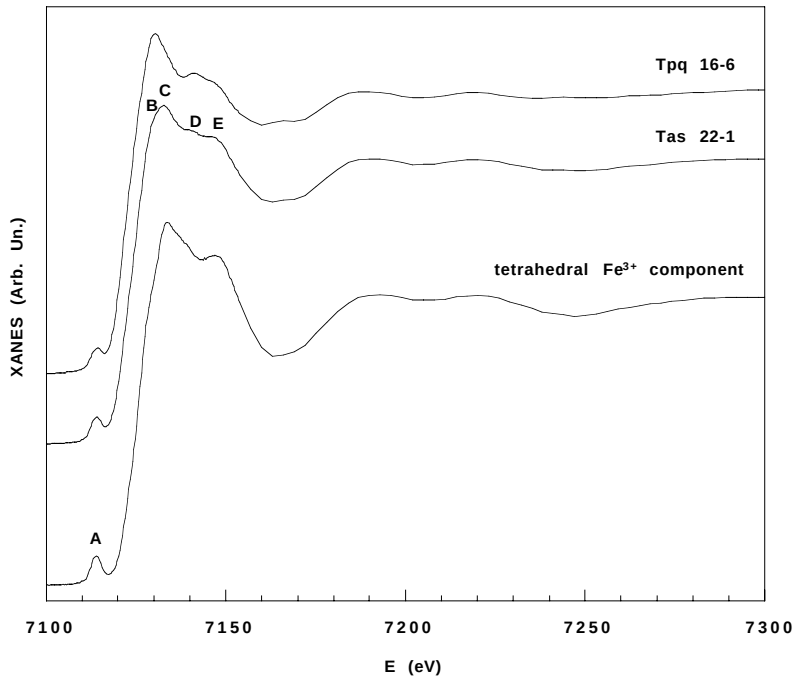

FIG. 5: Comparison between the Fe *K*-edge XANES spectra of micas containing Fe mainly in tetrahedral coordination (Tpq 16-6 = 0.79 and Tas 22-1 = 0.65 $^{[4]}Fe^{3+}/Fe_{tot}$, respectively). Bottom spectrum: tetrahedral Fe^{3+} component extracted by linear combination of the two previous spectra.

The shift (ca. 1 eV) observed in Fig. 5 between the Tas 22-1 and Tpq 16-6 Fe *K*-edges, may be correlated only to an effect of the tetrahedral component: as a matter of fact, the complete edge extracted from those two samples shows an even higher shift, because the most

intense octahedral structures located around 7130 eV contribute in different proportions to the different edge intensity rise observed in the two spectra.

For these micas the mean ⟨T-O⟩ bond distance is related to tetrahedral occupancy[2]. Thus, the substitution $^{[4]}Fe^{3+}\ ^{[4]}Al_{-1}^{3+}$, which links phlogopite with tetra-ferriphlogopite, increases the dimensions of the tetrahedral site and requires both the extension of the octahedral triads (*i.e.*, the unshared edges of octahedra) and the increase in distortion of the rings of tetrahedra (*i.e.*, α) so as to link the sheet of octahedra by the bridge of the O3 atom. Therefore, the differences in α value displayed by phlogopite (Phl Fr-1, $\alpha = 6.7°$) and tetra-ferriphlogopite (Tas 22-1, $\alpha = 11.5°$), two samples having similar octahedral site occupancies, may be related to differences in the amount of Fe^{3+} in the octahedral sites, which induces a relatively large sheet of tetrahedra in the tetra-ferriphlogopite crystal.

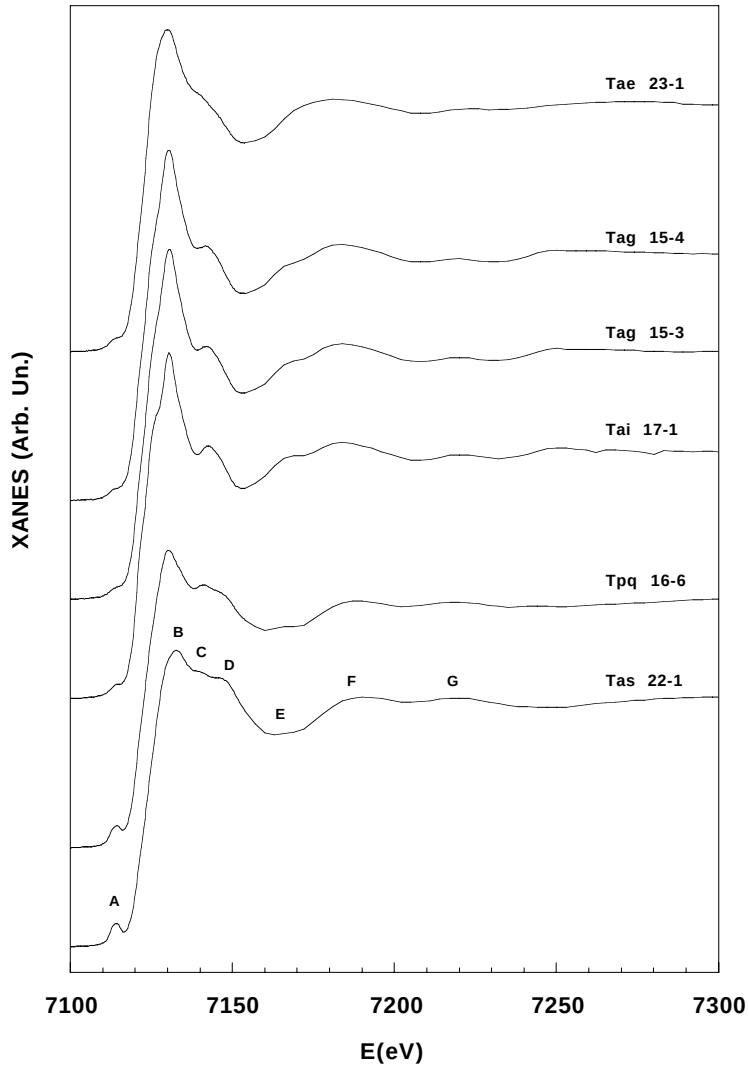

FIG. 6: Fe *K*-edge XANES spectra of trioctahedral micas containing iron in both T and O coordination. See text and Table 1 for details

In a tetra-ferriphlogopite, the misfit between octahedral and tetrahedral sheet, produced by the increase of the $\langle O - O \rangle_{basal}$ length, is recovered, in addition to by the α rotation, by an enlargement of the octahedral triads (*i.e.*, the unshared edges of octahedral *cis*- and *trans*-sites). In the end member phlogopite Phl Fr-1 the mean value of the octahedral triads is 3.051 Å whereas in the end member tetra-ferriphlogopite Tas 22-1 it increases to 3.097 Å[5]. Thus the $^{[6]}Fe^{2+}$ for $^{[6]}Mg$ exchange in the ferroan tetra-ferriphlogopite Tpq16-6 does not seem to produce relevant differences to the octahedral sheet geometry because the octahedron mainly reflect the tetrahedral topology instead of the local crystal chemistry.

We can now consider the problem of Fe in tetrahedral coordination in most general terms. Tas 22-1 and Tpq 16-6, our two model micas (Table 1) both exhibit the characteristically intense pre-edge feature A that warns for such a coordination (Fig. 6). However, the spectra of Fig. 6 are divided in three different pairs. The bottom pair consists of the two above-mentioned micas, which are characterised by the evident pre-edge, and by other features the most intense of which has the edge at about 7140 eV, to be seen best in Tas 22-1. The IMS region of these samples shows at least three features, large but well resolved. Tag 153 ,Tag 15-4 and Tai17-1represent the second set (middle): all shown a very small pre-edge A, and FMS and IMS regions that are even better resolved and intense. Finally, the Tae 23-1 sample is unique: it is an intermediate case where all XANES features present in the previous spectra are present but smoothed. This difference, when compared to the extracted pure tetrahedral Fe spectrum (Fig. 5), directly reflects the tetrahedral Fe concentration present in the micas. In addition, the Tae 23-1 spectrum, with its broadening of all features, suggests a high local structural disorder all around the photoabsorber.

4 CONCLUSIONS

The analysis of the XANES spectra of trioctahedral micas of end member as well as intermediate compositions along the phlogopite to annite and phlogopite to tetra-ferriphlogopite joins has confirmed the main assumption underlying our study:

the XANES spectra of complex minerals result from superimposition of simple spectra of atoms and ions recorded, and the individual contribution can be deconvoluted by careful analysis of model samples.

In the particular case of Fe in trioctahedral micas:

the characteristic features of Fe located in the tetrahedral sheet (sites) can be discriminated from those of Fe located in the octahedral sheet (sites);

octahedral Fe can be recognized and, to a certain extent resolved, when in the divalent vs. trivalent oxidation state;

only a complete examination and evaluation of the entire edge spectrum can solve the problem of iron partition among sites and oxidation states. Attempts resting on correlations between single parameters such as intensity and energy of individual peaks are bound to be limited to short extrapolation..

The results of XAS analysis compare well with those obtained by single crystal XRD refinement on the same mica samples, thus backing our suggestion that they can be generalized to all trioctahedral micas belonging to the phlogopite – annite - tetra-ferriphlogopite group.

Where the two conclusions diverge, this is due to the intrinsic properties of two methods: XRD averages on a long-range order while XAS details on local structures. This is a particularly evident in mica samples exhibiting high degree of structural disorder.

5 ACKNOWLEDGEMENTS

XAS measurements were carried out at SSRL synchrotron, which is operated by Stanford University on behalf of U.S. Department of Energy. Financial support to this study was granted by MURST (COFIN 1999 “Layer silicates: crystal chemical, structural and petrological aspects”) and by CNR (Coordinate project 1999 “Igneous and metamorphic micas”).

6 REFERENCES

(1) A.Bianconi, XANES Spectroscopy. In: “X-ray Absorption: Principles, Applications, Techniques of EXAFS, SEXAFS and XANES” (D.C. Konigsberger, R. Prins, Eds.), Wiley, New York, 573-662 (1988).

(2) M.F. Brigatti, , S. Guggenheim , Mica crystal chemistry and the influence of intensive variables on atomistic models. In: “Advances on Micas (Problems, methods, applications in Geodynamics)”, Accademia Nazionale dei Lincei, Roma, 2-3 November 2000, 29-56 (2000).

(3) M.F. Brigatti, A.E. Lalonde, L. Medici, Crystal chemistry of $^{[4]}Fe^{3+}$-rich phlogopites: a combined single-crystal X-ray and Mössbauer study. In: “Clays for our future”. Proceedings of the 11th International Clay Conference, Ottawa, Canada, 1997 (H. Kodama, A.R. Mermut, J.K. Torrance, Eds.). ICC97 Organising Committee, Ottawa, Canada, 317-327 (1999).

(4) M.F. Brigatti, C. Lugli, L. Poppi, E.E. Foord, D.E. Kile, American Mineralogist, **85**, 1275-1286 (2000).

(5) M.F. Brigatti, L. Medici, L. Poppi, Clays and Clay Minerals, **44**, 540-545 (1996).

(6) D.J.M. Burkhard, G.C. Ulmer, G. Redhammer, G.H. Myer, American Mineralogist, **84**, 493-505 (1999).

(7) D.M. Burt, Vector representation of phyllosilicate composition. In: “Hydrous phyllosilicates (exclusive of micas) (S.W. Bailey, Ed.). Reviews in Mineralogy, **19**, 561-600 (1988).

(8) G. Cruciani, P.F. Zanazzi, S. Quartieri, European Journal of Mineralogy, **7**, 255-265 (1995).

(9) J.S. Delaney, S., Bajt, S.R Sutton M.D. Dyar, In situ microanalysis of Fe^3/Fe ratio in amphibole by X-ray absorption near-edge structure (XANES) spectroscopy. In: “Mineral Spectroscopy, a tribute to Roger Burns” (M.D. Dyar, C. A. McCammon, M.W. Schaefer, Eds.). Geochemical Society, Special Publication, **5**, 289-304 (1995).

(10) G. Donnay, N. Morimoto, H. Takeda, J.D.H. Donnay, Acta Crystallographica, **17**, 1369-1373 (1964).

(11) G. Dräger, R. Frahm, G. Materlik, O. Brümmer, Physica Status Solidi (B), **149**, 287-294 (1988).

(12) M.D. Dyar, American Mineralogist, **72**, 102-112(1987).

(13) M.D. Dyar, American Mineralogist, **75**, 656-666 (1990).

(14) M.D. Dyar, Spectroscopy of iron in micas. In: "Advances on Micas (Problems, methods, applications in Geodynamics)", Accademia Nazionale dei Lincei, Roma, 2-3 November 2000, 65-80 (2000).
(15) M.D. Dyar, J.S. Delaney, S.R. Sutton, European Journal of Mineralogy, **13**, 1079-1098 (2001).
(16) M.D. Dyar, J.S. Delaney, S.R. Sutton, M.W. Schaefer American Mineralogist, **83**, 1361-1365 (1998).
(17) R.F. Dymek, American Mineralogist, **68**, 880-899 (1983).
(18) L.G. Farmer, A.I. Boettcher , American Mineralogist, **66**, 1154-1163 (1981).
(19) G. Giuli, E. Paris, Z.Y. Wu, M.F. Brigatti, G. Cibin, A. Mottana, A. Marcelli, European Journal of Mineralogy, **13**, 1099-1108 (2001).
(20) B.Güttler, W. Niemann, S.A.T. Redfern, Mineralogical Magazine, **53**, 591-602 (1989)
(21) R.M Hazen, C.W. Burnham, American Mineralogist, **58**, 889-900 (1973).
(22) R.M. Hazen, D.R. Wones, American Mineralogist, **57**, 103-129 (1972).
(23) S.M. Heald, J.E. Amonette, G.D. Turner, A.D. Scott, Physics B, **208-209**, 604-606 (1995).
(24) D. Heumann, G. Dräger, S. Bocharov . Journal de Physique -IV, **7 (C2)** Part 1, 481-483(1997).
(25) F.W. Lytle, R.B. Greegor, D.R. Sandstrom, E.C. Marques, J. Wong, C.L. Spiro, G.P. Huffman, F.E. Huggins : Nuclear Instrument and Methods in Physical Research, A **226**, 542-548 (1984).
(26) A. Manceau, D. Bonnin, P. Kaiser, C. Fretigny, Physics and Chemistry of Minerals, **16**, 180-185 (1988).
(27) A. Manceau, D. Bonnin, W.E.E. Stone, J.Sanz, Physics and Chemistry of Minerals, **17**, 363-370 (1990).
(28) R. Meyrowitz, Analytical Chemistry, **42**, 1110-1113 (1970).
(29) A. Mottana, A. Marcelli, G. Cibin, M.D. Dyar, X-ray absorption spectroscopy of the micas. In: "Advances on micas (Problems, methods, applications in Geodynamics)". Accademia Nazionale dei Lincei, Roma, 2-3 November 2000, 119-136 (2000).
(30) C.R. Natoli, Near edge absorption structure in the framework of the multiple scattering model. Potential resonance on barrier effects. In: "EXAFS and near edge structure" (A. Bianconi, L. Incoccia, S. Stipcich, Eds.) (Springer Series in Chemical Physics, Vol. 27). Berlin, Springer-Verlag, 43-47 (1983).
(31) C.R. Natoli, M. Benfatto, A unifying scheme of interpretation of X-ray absorption spectra based on multiple scattering theory. In "EXAFS and Near Edge Structure IV" (P. Lagarde, D. Raoux, J. Petiau, Eds.). Journal de Physique, **47-C8**, 11-23 (1986).
(32) C.R. Neal, L.A. Taylor, Mineralogy and Petrology, **40**, 207-224 (1989).
(33) D.G. Rancourt,M.Z. Dang, A.E. Lalonde, American Mineralogist, **77**, 34-93 (1992).
(34) C.R. Rebbert, E. Partin, D.A. Hewitt, American Mineralogist, **80**, 345-354 (1995).
(35) G.J. Redhammer, A. Beran, E. Dachs, G. Amthauer, Physics and Chemistry of Minerals, **20**, 382-394 (1993).
(36) M. Rieder, G. Cavazzini, Y.S. D'yakonov, V.A. Frank-Kamenetskii, G. Gottardi, S. Guggenheim, P.V. Koval ,G. Müller, A.M.R. Neiva, E.W. Radoslovich, J.L. Robert, F.P. Sassi, H. Takeda, Z. Weiss, D.R. Wones, Clays and Clays Minerals, **46**, 586-595 (1998).
(37) T.F. Semenova, I.V. Rozhdestvenskaya, V.A. Frank-Kamenetskii. Soviet Physics Crystallography **22**, 680-683 (1977).
(38) D. Virgo, R.K. PoppAmerican Mineralogist, **85**, 753-759 (2000).

(39) G.A Waychunas, M.J. Apted G.E. Brown Jr., X-ray K-edge absorption spectra of Fe minerals and model compounds near edge structure. Physics and Chemistry of Minerals, 10, 1-9. (1983).
(40) T.E. Westre, P. Kennepohl, J.G. DeWitt, B. Hedman, K.O. Hodgson, E.I.Solomon, Journal of the American Chemical Society, **119**, 6297-6314 (1997).
(41) M. Wilke, F. Farges, P.E. Petit, G.E. Brown Jr., F. Martin, American Mineralogist, **86**, 714-730 (2001).
(42) J. Wong, T. Tanaka, M. Rowen, F. Schaefers, R.B. Muller, Z.U. Rez, Journal of Synchrotron Radiation, **6**, 1086-1095 (1999).